Topics in Catalysis (2020) 63:1545–1556
https://doi.org/10.1007/s11244-020-01321-z

ORIGINAL PAPER

Reactivity and Stability of Ultrathin VO_x Films on Pt(111) in Catalytic Methanol Oxidation

Bernhard von Boehn[1] · Lena Scholtz[1,2] · Ronald Imbihl[1]

Published online: 31 July 2020

Abstract
The growth of ultrathin layers of VO_x (< 12 monolayers) on Pt(111) and the activity of these layers in catalytic methanol oxidation at 10^{-4} mbar have been studied with low-energy electron diffraction, Auger electron spectroscopy, rate measurements, and with photoemission electron microscopy. Reactive deposition of V in O_2 at 670 K obeys a Stranski–Krastanov growth mode with a $(\sqrt{3} \times \sqrt{3})R30°$ structure representing the limiting case for epitaxial growth of 3D-VO_x. The activity of VO_x/Pt(111) in catalytic methanol oxidation is very low and no redistribution dynamics is observed lifting the initial spatial homogeneity of the VO_x layer. Under reaction conditions, part of the surface vanadium diffuses into the Pt subsurface region. Exposure to O_2 causes part of the V to diffuse back to the surface, but only up to one monolayer of VO_x can be stabilized in this way at 10^{-4} mbar.

Keywords vanadium oxide catalysts · Pt(111) · Supported catalyst · Methanol oxidation · Stranski–Krastanow growth

1 Introduction

Vanadium oxides belong to the most important catalysts in chemical industry, finding applications for example in sulfuric acid production and in many partial oxidation reactions [1]. Typically the V-oxides are supported on oxidic materials like SiO_2, Al_2O_3, ZrO_2 or TiO_2 with the most active form being isolated VO_x-clusters or VO_x-films of monolayer thickness [2, 3]. Quantum chemical calculations and surface science experiments were able to clarify the reaction mechanism in catalytic methanol oxidation and the influence of the support material [4–8]. In the surface science approach [9], first single crystals of the bulk oxides were studied [10, 11], followed by planar model systems in which ultrathin V-oxide layers were deposited on single crystal oxide surfaces like α-Al_2O_3(0001), CeO_2(111) or TiO_2(110) [12–15] and on the fcc(111) und fcc(100) surfaces of the metals Pt, Rh, Pd, Cu, and Au [16–20]. In the past three decades the synthesis and characterization of ultrathin metal oxide films on metal surfaces has evolved into an own research field [21, 22].

A particularly well studied system are ultrathin V-oxide layers on a Rh(111) surface with the V coverage being in the monolayer and submonolayer range [20, 23, 24]. The dynamics of catalytic reactions on VO_x/Rh(111) have been studied with spatially resolving methods focusing on catalytic methanol oxidation. A very rich redistribution dynamics of the VO_x layer on Rh(111) was found with breathing VO_x islands in the 10^{-4} mbar range, turbulent dynamics at 10^{-2} mbar and, remarkably, with reaction-induced coalescence of macroscopic VO_x islands in the 10^{-4} mbar range [25, 26]. A natural question was how general the phenomenon of a reaction-induced island coalescence is, i.e., whether such ripening processes can also be observed in other reactions [27], with different support materials [28–30], and with other oxidic catalysts. It turned out that a number of oxidation reactions showed qualitatively the same behavior on VO_x/Rh(111) as long as O_2 is used as oxidizing agent [31].

Pt(111) is a fcc(111) noble metal surface similar to Rh(111), and therefore one should expect to find quite similar behavior on VO_x/Pt(111) as on VO_x/Rh(111). Different

Electronic supplementary material The online version of this article (https://doi.org/10.1007/s11244-020-01321-z) contains supplementary material, which is available to authorized users.

✉ Ronald Imbihl
imbihl@pci.uni-hannover.de

[1] Institut für Physikalische Chemie und Elektrochemie, Leibniz Universität Hannover, Callinstrasse 3A, 30167 Hannover, Germany

[2] Present Address: Division 1.2 Biophotonics, Bundesanstalt für Materialforschung und -prüfung (BAM), Richard-Willstätter-Str. 11, 12489 Berlin, Germany

from the system VO_x/Rh(111), which has thoroughly been characterized in the past two decades [20, 23, 24], only few experimental studies on the growth and reactivity of VO_x films on Pt(111) are reported in the literature [19, 32–34]. Here we report on the growth behavior of VO_x on Pt(111) and we investigate the catalytic activity and the dynamics of such a VO_x layer during catalytic methanol oxidation.

The concept of depositing oxides onto a metal support instead of having small metal particles sitting on an oxidic support, as it is the case for the supported catalysts used in industry, has been termed inverse model catalyst approach [22, 35–38]. Besides practical advantages such as avoiding electrical charging of the sample, this concept has been used to study processes at the metal/oxide interface, and to investigate a group of phenomena summarized under the term strong metal support interaction (SMSI). Historically, the term SMSI was introduced by Tauster who observed a change in the H_2 and CO adsorption properties after high temperature reduction of dispersed platin group metals (PGM) on metal oxide supports [39–41]. Transmission electron microscopy unambiguously showed the encapsulation of supported PGM catalysts by their metal oxide support [42–45]. Besides partial wetting or complete encapsulation of metallic nanoparticles by the oxidic support, also the formation of intermetallic compounds or alloys has been observed, especially at very high temperature under reducing conditions [46, 47].

In the present case, the inverse catalyst concept seems not to be adequate for VO_x/Pt(111) since V-oxide is not used as a support material for Pt particles. Nevertheless, the concept still appears to be useful to explore the interface VO_x/Pt and to compare the properties of ultrathin V-oxide layers on different noble metal surfaces. Surprisingly the system VO_x/Pt(111) displays quite different properties than the system VO_x/Rh(111) with respect to the structure as well as with respect to the catalytic activity, stability and dynamic behavior in catalytic methanol oxidation. The differences can be traced back to different properties of the VO_x film on Pt(111), and to a low oxygen adsorption energy and slow O_2 adsorption kinetics on Pt(111) [48–52].

2 Experimental

The experiments are performed in a standard ultrahigh-vacuum (UHV) vessel equipped with a photoemission electron microscope (PEEM), a low-energy electron diffraction (LEED) optics, a cylindrical mirror analyzer for Auger electron spectroscopy (AES), and a differentially pumped quadrupole mass spectrometer (QMS) for temperature programmed reaction (TPR) measurements. The Pt(111) single crystal (8 mm diameter, 1 mm thick) is spot-welded to two Ta wires. Heating the surface is either possible via passing current through the Ta wires (up to ~ 1100 K) or by electron bombardment from the sample backside. The temperature is measured with a K-type thermocouple spot-welded to the backside of the Pt crystal. Surface cleaning is performed by repeated cycles of Ar^+ ion sputtering (1 keV, 300 K, 2–5 µA, 20 min) and oxygen treatment at 1×10^{-6} mbar and 820–1020 K. Each cleaning cycle is finished by a final flash annealing to 1100 K prior to experiments. The presence of impurities is checked by AES. Vanadium oxide films are deposited by reactive evaporation [23], a process in which V is evaporated by electron beam bombardment from a high purity V rod (Goodfellow) in an oxygen atmosphere at elevated substrate temperature. VO_x is deposited at 670 K in an oxygen atmosphere of 2×10^{-7} mbar.

Under reaction conditions oxygen and methanol are dosed through high precision leak valves ensuring constant partial gas pressures via a feedback controlled gas inlet system. The pressure is measured with a Bayard-Alpert ionization gauge, (uncorrected pressure). To perform TPR measurements, the sample is positioned directly in front of a cone of 6 mm opening that connects the main UHV chamber to a differentially pumped QMS. In this way, all detected molecules have hit the sample surface prior to detection. To convert the ion currents measured in the QMS into pressure units, tabulated gas correction factors have been taken into account, as well as molecule fragmentation patterns. Ex situ sample characterization is carried out by AES and LEED prior and after exposure to methanol oxidation.

3 Results

3.1 Growth of VO_x on Pt(111)

The rate of VO_x deposition during reactive evaporation onto the Pt(111) substrate is followed by a combined AES and LEED analysis. VO_x is successively deposited, first in 30 s steps up to a total deposition time of 5.5 min, afterwards the deposition is continued in larger steps ranging between one and 10 min. Before and after each deposition step, the sample is kept for 10 min at evaporation conditions, i.e. at 670 K in 2×10^{-7} mbar oxygen. The growth of VO_x is monitored by AES and LEED after the sample has been cooled down to room temperature in the oxygen atmosphere. The AES deposition rate and a series of LEED images recorded throughout the deposition process are shown in Figs. 1 and 2, respectively.

The plot of the V, O, and Pt Auger intensities as a function of deposition time in Fig. 1 shows a steep, linear increase of the V and O signals during the first 2.5 min of VO_x deposition, accompanied by a sharp decrease of the Pt signal (for details please refer to the Online Resource 1). After 2.5 min the V and O signals continue to increase, but

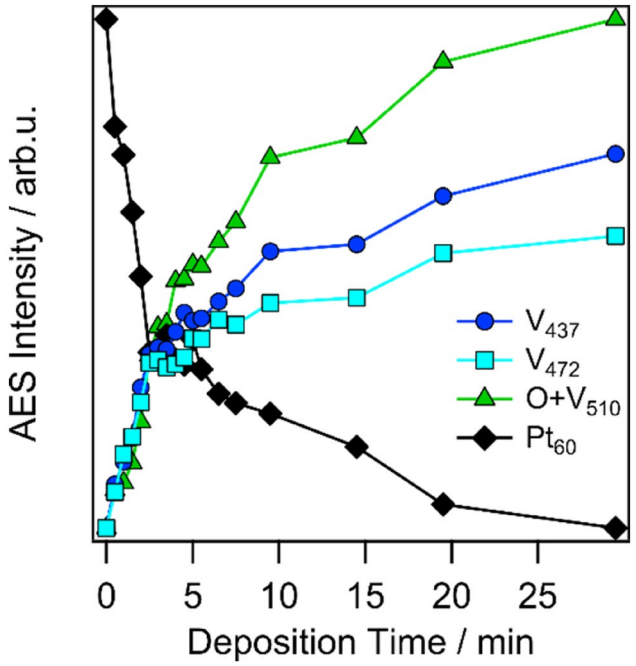

Fig. 1 Deposition rate calibration of VO_x on Pt(111) obtained by AES. Reactive evaporation of VO_x in 2×10^{-7} mbar O_2 at 670 K is applied. Shown are the peak to peak intensities of the V $L_{2,3}M_{2,3}M_{2,3}$ (V_{437}), V $L_{2,3}M_{2,3}M_{4,5}$ (V_{473}), V $L_{2,3}M_{4,5}M_{4,5}$ and O $KL_{2,3}L_{2,3}$ ($O+V_{510}$), and Pt (Pt_{60}) Auger transition. The corresponding spectra are acquired at room temperature in vacuum with a primary electron energy of 3 kV. Adapted with permission from [62]

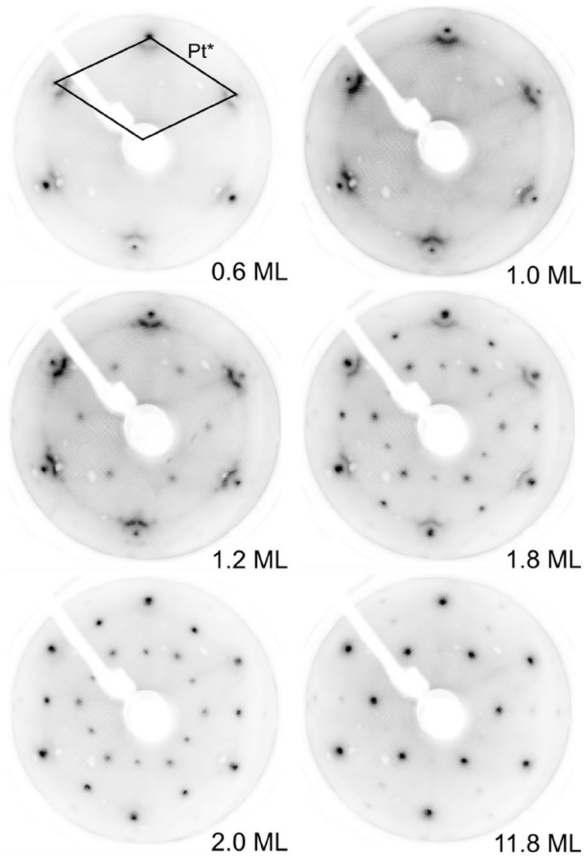

Fig. 2 LEED images acquired at 300 K in vacuo during stepwise reactive evaporation of VO_x. The data were recorded together with the AES calibration curve in Fig. 1. The VO_x coverages are relative coverages based on the calibration in Fig. 1. An electron energy of 65 eV was used for LEED, the reciprocal unit cell of the Pt substrate is indicated and labeled Pt* in the first LEED pattern. Adapted with permission from [62]

at a considerably lower rate. A similar change in slope can also be seen in the Pt signal, which decreases at a slower rate starting from 2.5 min. We interpret the initial linear increase followed by a pronounced change in the slope of the V and O signals as completion of the first oxide monolayer, followed by the growth of three-dimensional VO_x crystallites on top of the initial layer. Following arguments provided in the next two paragraphs, we conclude that during reactive evaporation VO_x grows in the Stranski–Krastanow mode [53, 54]. According to the AES calibration curve in Fig. 1, 2.5 min deposition time are required to deposit 1 ML of VO_x. The coverage of 1 ML refers to a closed VO_x film, i.e. we are using relative coverages. Since no structure model for the V-oxide film exists, the number of V atoms present on the surface is not known. Accordingly, VO_x coverages cannot be expressed in monolayer equivalents (MLE), as customary in studies on the growth of ultrathin oxide films.

The interpretation of the AES data as a Stranski–Krastanow growth mode of VO_x on Pt(111) is further corroborated by the LEED images shown in Fig. 2. Initially, a diffuse Moiré-type LEED pattern is observed for coverages below 1 ML. As the first oxide layer is completed, additional weak spots of a $(\sqrt{3} \times \sqrt{3})$R30° structure appear superimposed onto the Moiré pattern. Starting at around 1.4 ML, spots belonging to a (2×2) are added to the $(\sqrt{3} \times \sqrt{3})$R30° and the vanishing Moiré LEED spots. After the deposition of ~ 2 ML VO_x only the $(\sqrt{3} \times \sqrt{3})$R30° and (2×2) remain. Further VO_x dosage results in an intensity decrease of the (2×2) diffraction pattern, until at roughly 12 ML the $(\sqrt{3} \times \sqrt{3})$R30° diffraction pattern dominates and only very faint spots of the (2×2) remain visible in LEED.

We interpret the sequence of LEED patterns, in terms of a Stranski–Krastanow growth mode, as follows: For coverages up to 1 ML vanadium oxide grows as a poorly ordered 2D-oxide until the first monolayer is completed. Further VO_x dosage results in the nucleation and growth of small 3D-crystallites that exhibit a $(\sqrt{3} \times \sqrt{3})$R30° structure as topmost plane. The reason to assign the $(\sqrt{3} \times \sqrt{3})$R30° structure to 3D-crystallites is that the same $(\sqrt{3} \times \sqrt{3})$R30° structure is observed after the growth of a many monolayers thick VO_x film. The appearance of a (2×2) in LEED that follows is apparently due to a transformation of the 1st monolayer exhibiting a Moire type pattern. This can either be

caused by an ordering of the first oxide layer with increasing VO_x coverage, resulting from an incorporation of V atoms into the initial oxide layer as observed in the system VO_x/Rh(111) [23], or, alternatively, by opening up a second VO_x layer on areas not covered by the $(\sqrt{3} \times \sqrt{3})R30°$ crystallites. The growth mode would in that case no longer be pure Stranski–Krastanow. Finally, after deposition of a large amount of VO_x, only the $(\sqrt{3} \times \sqrt{3})R30°$ phase is present on the surface. From the Auger data we estimate an O/V ratio of roughly 1.4 for several layers thick VO_x films, in agreement with the composition of a V_2O_3 phase (for details please refer to the Online Resource 1).

3.2 Reaction Rate Measurements During Methanol Oxidation

For TPR measurements, the bare Pt(111) surface as well as VO_x/Pt(111) surfaces with different VO_x coverages (0.6 and 4 ML) are placed directly in front of a cone that connects the main chamber to a differentially pumped QMS. The reaction rate curves for Pt(111) and VO_x/Pt(111) during a heating/cooling cycle are shown in Figs. 3a and b, respectively. On the uncovered Pt(111) surface pronounced production peaks appear in the CO_2 and H_2O signals at 470 K (heating branch) and 440 K (cooling branch). Besides the product of total oxidation, CO_2, also traces of the partial oxidation product formaldehyde are found on the uncovered Pt(111) surface in a very broad production peak around 500 K. Only

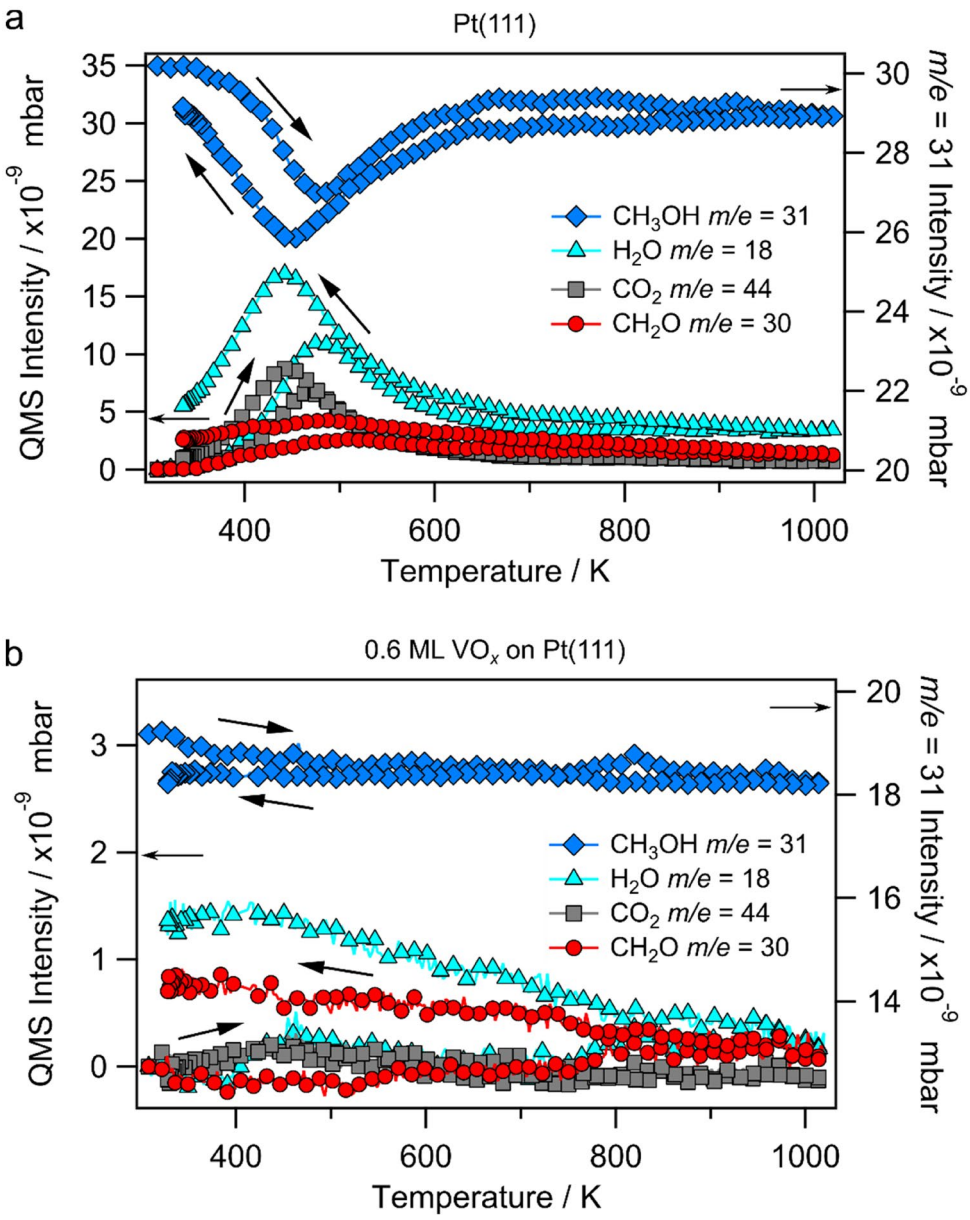

Fig. 3 TPR measurements (0.2 K/s) on Pt(111) **a** and 0.6 ML VO_x on Pt(111) **b** during catalytic methanol oxidation in the 10^{-4} mbar range. Shown are the methanol (right axis) and water, carbon dioxide and methanol (left axis) QMS signals as a function of temperature. Gas phase composition: 1×10^{-4} mbar oxygen and 1×10^{-5} mbar methanol. Adapted with permission from [62]

negligible catalytic activity is seen above ≈ 600 K. The low product formation at high temperature is probably caused by the low initial sticking coefficient of oxygen on Pt(111) of 0.05 at 300 K [55], which decreases with increasing temperature. Moreover, the surface residence time of adsorbates decreases with rising temperature. Interestingly, no CO signal can be found, i. e. it is below the detection limit of the mass spectrometer.

The deposition of larger quantities of VO_x onto Pt(111) inhibits almost all catalytic activity, as evidenced by rate measurements with 0.6 and 4 ML VO_x. The data in Fig. 3b show reaction rates that are more than one order of magnitude lower than on the uncovered Pt(111) surface. The increase in the rate signals at lower temperature are probably caused by a slightly unstable gas flow and by accumulation of H_2O in the UHV chamber. Thermal decomposition of methanol at hot filaments causes some background signal. This low activity does not change if the gas phase composition is modified to more reducing conditions with $p(CH_3OH)$ being 5×10^{-5} mbar and 1×10^{-4} mbar, respectively, while keeping $p(O_2)$ constant at 1×10^{-4} mbar. Evidently, the deposition of thin VO_x films passivates the Pt(111) surface with respect to methanol oxidation.

LEED and AES data acquired before and after exposure to reaction conditions are shown in Fig. 4 for 0.6 and 4 ML thick VO_x films. Auger spectra are recorded before and after a heating/cooling cycle in a gas atmosphere of oxygen and methanol. One notices a clearly detectable loss in V intensity as a consequence of the high temperature treatment. The V loss shows some dependence on the methanol to oxygen partial pressure ratio but the signal decrease varies strongly with the initial VO_x coverage. Whereas the loss in V_{437} intensity only amounts to 20–30% for the 0.6 ML films, more than 70% of the initial V intensity are lost after a 4 ML VO_x film was exposed to methanol oxidation. For the thin 0.6 ML films, the highest V loss is observed in a reducing gas atmosphere, i.e. with 1×10^{-4} mbar methanol and 1×10^{-4} mbar oxygen. The loss of V intensity is an indication for a migration of V atoms into the surface or subsurface region of the Pt crystal. Since such a formation of a subsurface V/Pt

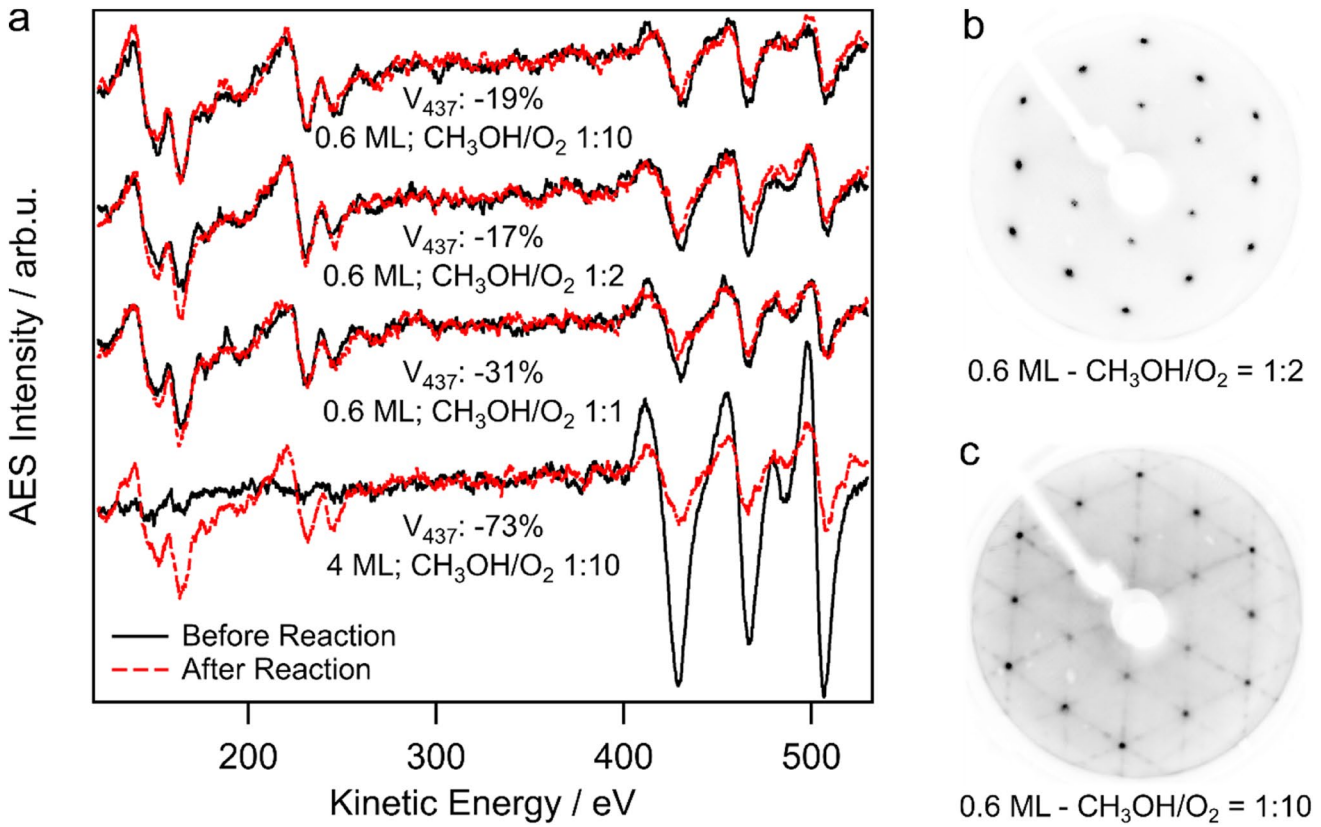

Fig. 4 Auger spectra and LEED images recorded before and after freshly deposited VO_x films on Pt(111) were exposed to catalytic methanol oxidation with varying CH_3OH to O_2 ratios. Reaction conditions are in the 10^{-4} mbar range. For methanol oxidation, the samples are heated with 0.2 K/s from 300 to 1020 K and back to room temperature in an atmosphere consisting of 1×10^{-4} mbar oxygen and methanol pressures of 1×10^{-5}, 5×10^{-5} and 1×10^{-4} mbar, respectively. **a** Auger spectra recorded before (black solid line) and after (red dashed line) the reaction. The spectra were recorded with 3 keV primary electron energy. **b–c** LEED images (65 eV) recorded after 0.6 ML VO_x on Pt(111) were exposed to 1×10^{-4} mbar oxygen and either 5×10^{-5} mbar **b** or 1×10^{-5} mbar methanol **c**. In **c** a (2×2) superimposed with a $(1 \times n)$ pattern ($n = 8$,) with three rotational domains is visible. Adapted with permission from [62]

alloy requires metallic V, a reduction of VO_x is a necessary prerequisite for this process.

LEED shows an intense (2 × 2) after methanol oxidation on a 0.6 ML VO_x film with a 1:2 ratio of methanol and oxygen in the gas phase. A (2 × 2) is also obtained with a 1:10 methanol to oxygen ratio. Under more oxidizing conditions, however, additional spots of a (1 × *n*) structure (*n* = 8) appear in LEED, as shown in Fig. 4c. As shown below, a (2 × 2) also develops after several ML thick VO_x films are exposed to reducing conditions. The formation of a (2 × 2) accordingly depends on the gas phase composition, but to a minor degree on the initial VO_x coverage.

3.3 Segregation Behavior of VO_x/Pt(111)

Quite general, elevated temperatures favor the formation of alloys between the supporting metal and metal from the deposited metal oxide film. This is particularly true if no miscibility gaps exist in the phase diagram of the two metals, as it is the case for Pt/V [56]. In order to determine up to which temperature VO_x is stable as an oxide on the Pt(111) surface, a roughly 1.5 ML thick vanadium oxide film on Pt(111) is heated up to 1000 K in vacuum, while monitoring the surface composition with AES. Prior to this alloying experiment, the initially 5 ML thick VO_x/Pt(111) sample has been exposed to methanol oxidation and heated in 1×10^{-4} mbar oxygen at 870 K for 40 min. The resulting V, O and Pt signal vs. temperature curves recorded during heating the sample up in vacuum are shown in Fig. 5.

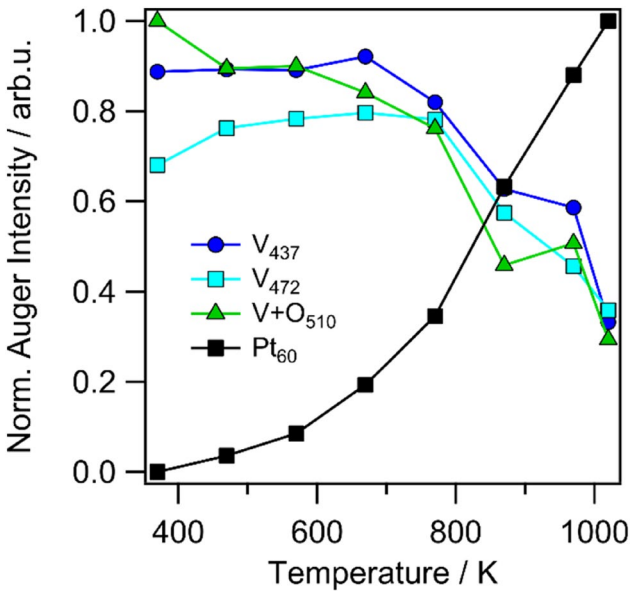

Fig. 5 Thermal stability of VO_x on Pt(111). The VO_x/Pt(111) sample ($\theta_{VOx} \approx 5$ ML) is heated in 100 K steps from 300 to 1020 K. Every 100 K an Auger spectrum is acquired (20 min acquisition time) at constant temperature before the sample is heated to the next temperature within about 2 min. Shown are the normalized V, O (left axis) and Pt (right axis) intensities as a function of sample temperature. Adapted with permission from [62]

Below 770 K the V and O Auger signals are constant, as can be seen in Fig. 5. A pronounced decrease in the V and O signals occurs beyond 770–870 K, accompanied by a growth of the Pt peak. We interpret the V and O intensity decrease as a reduction of VO_x followed by diffusion of V into the subsurface region of the Pt crystal (for details please refer to the Online Resource 1). The increase in the Pt signal that already starts beyond 400 K might be due to ordering processes in the VO_x layer. At 1020 K the V intensity has decreased by a factor of two compared to the initial V signal. After annealing the VO_x/Pt(111) sample for another 20 min at 1020 K, the V signal has only about 20% of the initial intensity at room temperature. The high temperature of 1020 K that is required to generate such a loss indicates a slow diffusion of V into the Pt crystal.

An alternative explanation for the decreasing V Auger signals under reducing conditions could also be an agglomeration of the initially homogeneously distributed VO_x into three-dimensional clusters. A similar behavior, the aggregation of a thin Ni/NiO layer into small, three-dimensional NiO clusters under oxidizing conditions has recently been observed in the $H_2 + O_2$ reaction over Ni/Rh(111) [57, 58]. However, if such a mechanism would operate in the VO_x/Pt(111) system, a V signal decrease would occur under oxidizing conditions and not under reducing conditions as observed here.

3.4 Stability of Submonolayer VO_x Films During Catalytic Methanol Oxidation

The reaction-induced redistribution dynamics of 0.4 and 5 ML VO_x supported on the Pt(111) surface are studied in the 10^{-4} mbar range with PEEM. A 0.4 ML VO_x film is heated in 1×10^{-4} mbar oxygen to 870 K within a few minutes, followed by introducing methanol into the vacuum chamber. As $p(CH_3OH)$ is varied in a wide pressure range between 1×10^{-5} and 1×10^{-4} mbar, no V-oxide redistribution is observed and the surface remains homogeneous in PEEM. Only gradual and homogeneous brightness changes are seen, reflecting a change in the work function. The observed brightness variations are indirectly linked to the adsorption of methanol and oxygen from the gas phase, which cause a reduction/oxidation of the VO_x overlayer. A higher amount of methanol in the gas phase results in an increased brightness due to the lower work function of adsorbed carbon containing species and of a reduced VO_x layer. With a lower methanol content in the gas phase, the VO_x film gets re-oxidized again, and C containing species desorb/react off, resulting in a higher work function and low PEEM intensity.

This result is in strong contrast to the systems VO_x/Rh(111) and VO_x/Rh(110), where a dynamic response and different redistribution patterns were observed [25, 28]. In order to systematically probe the accessible parameter range, linear heating/cooling ramps between 300 and 1020 K (0.2 K/s) are applied to 0.4 and 5 ML VO_x films on Pt(111). The composition of the atmosphere is varied between a 1:10 and a 1:1 ratio of p(MeOH)/$p(O_2)$, with $p(O_2)$ being kept fixed at 1×10^{-4} mbar. In these experiments no V-oxide island formation or other reaction dynamics are seen in PEEM.

3.5 Stability of Multilayer VO_x Films During Catalytic Methanol Oxidation

Since a diffusion of V into the Pt bulk only takes place under reducing conditions, the question is whether this process can be reverted by changing the oxygen coverage. This problem we address in the following with LEED and AES exposing VO_x films of different coverage to methanol oxidation in the 10^{-4} mbar range.

Figure 6 shows Auger spectra after a 5 ML VO_x film on Pt(111) has been exposed to methanol oxidation in the 10^{-4} mbar range with a p(MeOH)/$p(O_2)$ ratio of 1:10. AES data are also taken after a subsequent oxygen treatment at 870 K and $p(O_2) = 1 \times 10^{-4}$ mbar. The resulting Auger ratio V_{437}/Pt_{237} is reproduced in Fig. 6b. Initially, after reactive evaporation of 5 ML VO_x, LEED displays a diffuse $(\sqrt{3} \times \sqrt{3})R30°$ pattern shown in Fig. 6c. The corresponding Auger spectrum is dominated by V and O Auger transitions. After the sample has been exposed to catalytic methanol oxidation for roughly 40 min, the $(\sqrt{3} \times \sqrt{3})R30°$ structure has vanished and LEED displays a sharp (2 × 2) as demonstrated by Fig. 6d. In AES the V and O intensities are significantly decreased while the Pt related transitions grew in intensity. Evidently, even with oxygen being in large excess and with an oxygen pressure of 1×10^{-4} mbar, the oxygen coverage does not suffice to stabilize a 5 ML thick VO_x film during methanol oxidation.

In order to check for the reversibility of V bulk diffusion the VO_x/Pt(111) surface is, after the reaction treatment, exposed to 1×10^{-4} mbar oxygen at 870 K for 40 min. This results in a (1 × 1) with strong background intensity and streaky features around the integral order diffraction spots. In AES only a small part of the initial V and O intensity is restored, as shown in Fig. 6b. Apparently only a small amount of V atoms in subsurface sites can migrate back to the surface despite an elevated temperature and high oxygen partial pressure.

We obtain more insight as we systematically study the reversibility of V bulk diffusion for different V coverages. We subject four VO_x films with V coverages between 2 and 10 ML to a similar procedure of exposure to reaction conditions followed by oxygen treatment as described above. The reactions were carried out with varying methanol partial pressures, the oxidation step was always carried out at 870 K in 1×10^{-4} mbar oxygen. Surprisingly, the 40 min oxygen treatment at 870 K restores more or less the same V_{437}/Pt_{237}

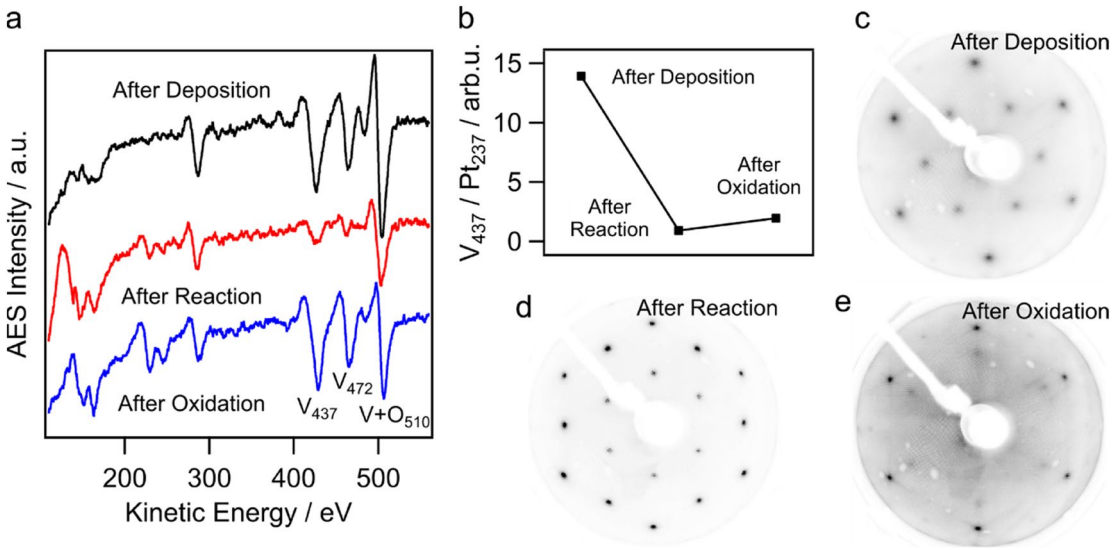

Fig. 6 Reaction induced V diffusion into the Pt bulk of 5 ML VO_x on Pt(111) during methanol oxidation and O induced V segregation. **a** Auger spectra recorded after deposition of 5 ML VO_x, after the sample was heated from room temperature to 1020 K (0.2 K/s) in 1×10^{-5} mbar methanol and 1×10^{-4} mbar oxygen, and after subsequent oxygen treatment at 870 K and 1×10^{-4} mbar. **b** V_{437}/Pt_{237} Auger intensity ratio measured after deposition, reaction and oxygen treatment. **c**–**e** LEED images (65 eV) recorded after deposition, reaction and oxidation, respectively. Adapted with permission from [62]

intensity ratio for all four films, irrespective of the initially deposited VO_x coverage. We compare these data with V_{437}/Pt_{237} Auger intensity ratios of the calibration curve of Fig. 1. For the four thick films exposed to reducing reaction conditions the values only vary within a small range; the average V_{437}/Pt_{237} intensity ratio is 1.6 ± 0.3. This value lies between the V_{437}/Pt_{237} intensity ratios of 0.8 and 1.2 ML films in Fig. 1, which are 1.2 ± 0.1 and 2.2 ± 0.1, respectively. A simple assumption to explain these findings is that only a certain amount of V dissolved in the Pt bulk can segregate back to the surface under oxidizing conditions until a closed oxide monolayer has been formed.

4 Discussion

4.1 VO_x Growth on Pt(111)

VO_x on Rh(111) [20, 23, 24] and on Pd(111) [17, 59–61] are systems where the structures developing in the submonolayer and monolayer range have been particularly well studied and understood. They represent two-dimensional VO_x network structures formed from VO_n polyhedra ($n = 3$–6) that are connected by sharing oxygen corner atoms [20]. In the multilayer range most of the structures that form on metal single crystal surfaces can be described as epitaxial growth of known bulk oxides of vanadium; VO(111) on Cu(100) and Ni(110) [62], V_2O_3(0001) on W(110) and Au(111) [63] and V_2O_5(001) on Au(111) [64, 65]. In the latter case an oxygen partial pressure of 50 mbar was applied to stabilize V in a +5 oxidation state. Typically, the growth of ultrathin transition metal oxide films on noble metal surfaces is kinetically controlled, and the preparation procedure has a decisive influence on the oxide phases that are formed [22].

The growth of VO_x on Pt(111) has only been investigated by few groups [19, 32–34]. With vibrational spectroscopy and LEED as main methods, Tang et al. studied the deposition of VO_x onto Pt(111) up to a thickness of three monolayers. Their results differ significantly from ours, but the differences can be attributed to the different preparation procedures used in both cases. Tang et al. deposited V at room temperature in vacuum and post-oxidized the surface at 623 K in 1×10^{-7} mbar O_2, whereas we deposited V by reactive evaporation at 670 K in an oxygen atmosphere of 2×10^{-7} mbar. In their calibration curve of VO_x deposition they observed two break points in the slope and concluded layer-by-layer growth up to three ML. A (2×2) developed only beyond 0.5 ML, for coverages > 2 ML, a $(3\sqrt{3} \times 6)$ was present. In particular the $(\sqrt{3} \times \sqrt{3})R30°$ that was the dominant structure in our experiments beyond 2 ML here, was not seen at all.

A (2×2) structure was seen after deposition of submonolayer VO_x films on Pd(111); it was described there as a VO wetting layer also denoted as s-V_2O_3 [17]. Based on their vibrational data Tang et al. followed the interpretation of the (2×2) as a surface V_2O_3 layer. Different from the results reported by Tang et al. we observed a (2×2) only in coexistence with a $(\sqrt{3} \times \sqrt{3})R30°$ structure after deposition of more than 1 ML (step-wise deposition) during VO_x growth. Furthermore we observed the (2×2) after methanol oxidation has been carried out on VO_x films of an initial thickness varying between 0.6 and several ML. From AES we estimate the VO_x coverage of the (2×2) obtained after reaction conditions were applied to thick VO_x films to be roughly 1 ML.

A $(\sqrt{3} \times \sqrt{3})R30°$ structure reported for thick VO_x layers ($\gtrapprox$1 MLE VO_x) on Rh(111) and Pd(111) was assigned to the (0001) oriented surface of corundum V_2O_3 [17, 23]. Accordingly, we attribute the $(\sqrt{3} \times \sqrt{3})R30°$ structure observed here to three-dimensional crystallites of V_2O_3 with (0001) orientation. Interestingly, no such corundum V_2O_3 phase has been reported by Tang et al. for VO_x/Pt(111). Although some weak $(\sqrt{3} \times \sqrt{3})R30°$ diffraction spots were visible after deposition of 2.5 ML VO_x on Pt(111) (Fig. 3f in [32]) they were not discussed further. For V coverages between 1 and 2 ML, a $(3\sqrt{3} \times 6)$ pattern was observed by Tang et al. who interpreted this pattern as a bilayer structure.

To conclude, compared with the results of Tang et al., we find differences in the growth mode—Stranski–Krastanow vs. layer-by-layer—as well in the structures at higher V coverage. Since different preparation procedures have been used the results are not in contradiction to each other. One could speculate whether the structures seen here are closer to thermodynamic equilibrium since reactive evaporation at high temperature was applied instead of post-oxidation. This, however, needs to be verified by future analyses.

4.2 Catalytic Activity of VO_x/Pt(111)

In catalytic methanol oxidation the system VO_x/Rh(111) exhibited a high catalytic activity and displayed remarkable dynamic behavior [25, 31], whereas VO_x/Pt(111) showed negligible catalytic activity and practically no dynamics at all. In this comparison we refer to submonolayer coverages of VO_x and reaction conditions in the 10^{-4} mbar range. If we take the picture of VO_x islands acting as catalytic microreactors on Rh(111), then we can explain the lower activity of VO_x/Pt(111) in two ways: (i) the VO_x islands are less active on Pt(111) and/or (ii) the surrounding metal surface, which in the case of Rh(111) provides the oxygen for the reaction, is less active in O_2 adsorption.

Starting with point (ii), Rh(111) has a high oxygen sticking coefficient as evidenced by a value of 0.3 at 300 K [49]. On Pt(111) where oxygen sticking reportedly is controlled by the step density, values around 0.06 are found for 300 K in the literature [48]. Evidently oxygen adsorption is much slower on Pt(111) as compared to Rh(111). Accordingly,

a considerable stationary O_{ad} coverage around 0.2 ML on the Rh surface has been measured with XPS, even at high temperature during methanol oxidation [25]. On Pt(111) the stationary oxygen coverage is expected to be very low under reaction conditions, even with a ten times excess of oxygen in the gas phase. Therefore under conditions where the supply of oxygen is rate-limiting, the rate of catalytic methanol oxidation will be small on VO_x/Pt(111).

Besides the low oxygen sticking coefficient on Pt(111), also the adsorption energies of oxygen on Pt(111) and Rh(111) differ considerably. The adsorption energy of atomic oxygen on Pt(111), as determined from thermal desorption spectroscopy (TDS), gives a value of 2.21 eV per O_2 molecule [48, 50]; with microcalorimetry a substantially larger energy of 3.16 eV was obtained [51]. DFT calculations for O/Pt(111) yield 2.68 eV for the adsorption energy at low O coverages ($\theta_O \leq 0.25$ ML) [52], surface vibrational gas-phase enthalpy corrections reduce this value to 2.46 eV, which is close to the experimental TDS adsorption energy. In contrary, DFT calculations for O/Rh(111) yield with 4.48 eV [66] and 4.88 eV [67] adsorption energies that are considerably above those for O/Pt(111).

Apparently, for an oxygen atom bonded to vanadium, it should be easier to change to a Rh site than to a Pt site because the energetic difference is smaller. Therefore, besides the kinetic factor given by different oxygen sticking coefficients, also a thermodynamic factor exists favoring oxygen exchange between VO_x and a Rh(111) surface as compared to VO_x and a Pt(111) surface. Oxidation reactions over VO_x catalysts proceed via a Mars-van Krevelen mechanism [68, 69], but the catalytic studies are typically conducted at high pressure (mbar to bar). At low pressure, reoxidation of VO_x by direct adsorption from the gas phase is presumably too slow to be efficient, and the effect of the supporting noble metal surface becomes important [25].

For V-oxide to be highly active in catalytic methanol oxidation, vanadyl groups should be present on the oxide surface [5, 6, 70–72]. Although Tang et al. demonstrated the existence of vanadyl containing V-oxide clusters on Pt(111) for coverages below 0.5 ML, these clusters condense into the (2×2) s-V_2O_3 structure already upon CO adsorption at room temperature [32]. The formation of vanadyl containing vanadium oxide on Pt(111) requires oxygen partial pressure in the mbar range [32]. This is confirmed by an infrared reflection absorption spectroscopy (IRAS) study of propane oxidation over VO_x/Pt(111) where the high activity in the mbar range was linked to the presence of vanadyl groups [34]. Given that no vanadyl groups are present on VO_x/Pt(111) in the 10^{-4} mbar range, the VO_x should exhibit only a small activity in catalytic methanol oxidation.

The island movement on VO_x/Rh(111) proceeds via a polymerization/depolymerization (PD) mechanism in which V_nO_m clusters are detached from the VO_x island in regions of high oxygen coverage and are reattached to the island in areas of low oxygen coverage [25]. With a low oxygen coverage and with no or only very shallow oxygen gradients that can evolve due to a negligible catalytic activity on VO_x/Pt(111), the PD mechanism cannot be effective on VO_x/Pt(111). A high oxygen sticking coefficient and adsorption energy of the metal surface alone, is not the only criterion to observe coalescence of VO_x islands. On Rh(110) the oxygen sticking coefficient is even larger than on Rh(111), but no island coalescence on VO_x/Rh(110) has been observed under reaction conditions [28, 29, 73]. However, the rate of formaldehyde production on VO_x/Rh(110) in catalytic methanol oxidation has been very low likewise, and one can speculate whether it is the absence of vanadyl groups also in this case that is responsible for the low activity of VO_x on Rh(110). In contrast to VO_x/Pt(111), however, a very rich dynamics was observed in catalytic methanol oxidation on VO_x/Rh(110): chemical wave patterns [30] and also VO_x island formation [28] were seen but no VO_x island coalescence.

4.3 Segregation Behavior of VO_x/Pt(111)

Under reaction conditions in the 10^{-4} mbar range, part of the vanadium on the surface starts to diffuse into the Pt bulk at temperatures above 770–870 K. Apparently, as a consequence of the low oxygen sticking coefficient and the low adsorption energy of oxygen on Pt(111), the oxygen coverage is not high enough to stabilize V as a surface oxide under reaction conditions. If the surface is then exposed to 1×10^{-4} mbar oxygen at 870 K for prolonged time, part of the V dissolved in the Pt bulk segregates back to the surface, forming (2×2) structure. However, the amount of V which can segregate back to the Pt surface is limited to approximately one monolayer of VO_x. A similar behavior has also been observed in the system VO_x/Rh(110), in which only a certain amount of VO_x could be stabilized by oxygen, while excess V diffused into the Rh bulk [74]. For comparison, on Rh(111) already oxygen pressures in the 10^{-7} mbar range suffice to stabilize VO_x on the surface up to 1000 K [24].

The high stability of VO_x/Rh(111) against reduction, and the diffusion of V into Pt subsurface sites even in the presence of oxygen at high temperature might be explained by thermodynamics. We have found that oxidizing conditions can stabilize ≈ 1 ML VO_x on Pt(111). This indicates that the Pt substrate is not able to supply enough oxygen to form strong Pt-O-V bonds, probably due a lower O-Pt bond strength as compared to Rh-O. This conclusion is supported by the observation that Rh-O-V bonds are a common structural motif in the system VO_x/Rh(111).

After adsorbed oxygen attracted V from the Pt bulk or from the subsurface region, a (2×2) structure is visible in LEED. The same pattern is seen if methanol oxidation is carried out under reducing conditions. We have assigned

this (2 × 2) to a V_2O_3 surface oxide known from the system VO_x/Pd(111) [75]. In the s-V_2O_3 structure V is directly bound to the Pd substrate. The oxygen binding energy on Pd(111) is ~ 1.5 eV, as calculated with DFT, and therefore much lower than for O/Rh(111) [76]. The low O binding energies on Pt and Pd might be the reason for the formation of M-V bonds (M = substrate metal), rather than M–O–V bonds as it is the case for VO_x/Rh(111).

With a metal oxide being reduced and being alloyed with the support metal, this process can be summarized under SMSI. However, one has to be aware that the system VO_x/Pt(111) represents an inverse model catalyst and not the actual supported catalyst used in industrial catalysis. Since the concept of inverse supported catalysts has also been applied to design novel type of catalysts, knowledge of the processes encountered here with VO_x/Pt(111) might be useful for constructing such catalysts [38].

5 Conclusions

We studied the growth and the catalytic activity of ultrathin layers of V-oxide on Pt(111) with coverages in the submonolayer and multilayer range (< 12 ML). We interpret the LEED/AES data during reactive V deposition as Stranski–Krastanow growth with the $(\sqrt{3} \times \sqrt{3})R30°$ structure as limiting case for thick films. The $(\sqrt{3} \times \sqrt{3})R30°$ structure presumably represents the (0001) plane of epitaxially grown 3D-crystallites of "corundum" V_2O_3. Significant differences to reports in the literature indicate that the growth mode as well as the resulting structures depend strongly on the preparation procedure. The activity of VO_x/Pt(111) is very low in catalytic methanol oxidation, what can be attributed to (i) a low O_2 sticking coefficient and a low oxygen adsorption energy of Pt(111) and (ii) to the absence of vanadyl groups in the VO_x layer in the 10^{-4} mbar range. No redistribution dynamics in the VO_x layer was detected during methanol oxidation in the 10^{-4} mbar range. Multilayer V-oxide coverages cannot be stabilized on the Pt(111) surface under reaction conditions in the 10^{-4} mbar range as part of the V, after being reduced, diffuses into the Pt bulk. Exposure to O_2, reverses the bulk diffusion, but only up to 1 ML of VO_x can be stabilized on the surface at 10^{-4} mbar.

Acknowledgements Open Access funding provided by Projekt DEAL. Bernhard von Boehn would like to thank the Department of Inorganic Chemistry of the Fritz Haber Institute of the Max Planck Society for financial support.

Compliance with Ethical Standards

Conflict of interest The authors declare no competing financial interest.

References

1. Grzybowska-Świerkosz B, Trifirò F (1997) Preface. Appl Catal A: Gen 157(1–2):1–2. https://doi.org/10.1016/S0926-860X(97)80165-2
2. Wachs IE, Weckhuysen BM (1997) Structure and reactivity of surface vanadium oxide species on oxide supports. Appl Catal A: Gen 157(1–2):67–90. https://doi.org/10.1016/S0926-860X(97)00021-5
3. Wachs IE (2013) Catalysis science of supported vanadium oxide catalysts. Dalton Trans 42(33):11762–11769. https://doi.org/10.1039/c3dt50692d
4. Göbke D, Romanyshyn Y, Guimond S et al (2009) Formaldehyde formation on vanadium oxide surfaces V_2O_3(0001) and V_2O_5(001): how does the stable methoxy intermediate form? Angew Chem Int Ed Engl 48(20):3695–3698. https://doi.org/10.1002/anie.200805618
5. Romanyshyn Y, Guimond S, Kuhlenbeck H et al (2008) Selectivity in methanol oxidation as studied on model systems involving vanadium oxides. Top Catal 50(1–4):106–115. https://doi.org/10.1007/s11244-008-9114-z
6. Döbler J, Pritzsche M, Sauer J (2005) Oxidation of methanol to formaldehyde on supported vanadium oxide catalysts compared to gas phase molecules. J Am Chem Soc 127(31):10861–10868. https://doi.org/10.1021/ja051720e
7. Ganduglia-Pirovano MV, Popa C, Sauer J et al (2010) Role of ceria in oxidative dehydrogenation on supported vanadia catalysts. J Am Chem Soc 132(7):2345–2349. https://doi.org/10.1021/ja910574h
8. Kropp T, Paier J, Sauer J (2014) Support effect in oxide catalysis: methanol oxidation on vanadia/ceria. J Am Chem Soc 136(41):14616–14625. https://doi.org/10.1021/ja508657c
9. Surnev S, Ramsey MG, Netzer FP (2003) Vanadium oxide surface studies. Prog Surf Sci 73(4–8):117–165. https://doi.org/10.1016/j.progsurf.2003.09.001
10. Goering E, Müller O, Klemm M et al (1997) Angle dependent soft-X-ray absorption spectroscopy of V_2O_5. Philos Mag B 75(2):229–236. https://doi.org/10.1080/13642819708202311
11. Goering E, Schramme M, Müller O et al (1997) Angular-resolved photoemission on V_2O_3 and VO_2. Phys B: Condens Matter 230–232:996–998. https://doi.org/10.1016/S0921-4526(96)00782-X
12. Artiglia L, Agnoli S, Granozzi G (2015) Vanadium oxide nanostructures on another oxide: the viewpoint from model catalysts studies. Coord Chem Rev 301–302:106–122. https://doi.org/10.1016/j.ccr.2014.12.015
13. Biener J, Bäumer M, Madix RJ et al (1999) A synchrotron study of the growth of vanadium oxide on Al_2O_3(0001). Surf Sci 441(1):1–9. https://doi.org/10.1016/S0039-6028(99)00728-1

14. Wong GS, Vohs JM (2002) An XPS study of the growth and electronic structure of vanadia films supported on CeO_2(111). Surf Sci 498(3):266–274. https://doi.org/10.1016/S0039-6028(01)01761-7
15. Wang Q, Madix RJ (2002) Partial oxidation of methanol to formaldehyde on a model supported monolayer vanadia catalyst: vanadia on TiO_2. Surf Sci 496(1–2):51–63. https://doi.org/10.1016/S0039-6028(01)01600-4
16. Kishi K, Hirai K, Yamamoto T (1993) XPS and XAES study for oxidation of V/Cu(100) and V, Na/Cu(100) surfaces. Surf Sci 290(3):309–318. https://doi.org/10.1016/0039-6028(93)90715-V
17. Leisenberger FP, Surnev S, Vitali L et al (1999) Nature, growth, and stability of vanadium oxides on Pd(111). J Vac Sci Technol, A 17(4):1743–1749. https://doi.org/10.1116/1.581884
18. Niehus H, Blum R-P, Ahlbehrendt D (2003) Structure of vanadium oxide (V_2O_3) grown on Cu_3Au(100). Surf Rev Lett 10(02n03):353–359. https://doi.org/10.1142/s0218625x03004962
19. Petukhov M, Rizzi GA, Granozzi G (2001) Spectroscopic and structural characterisation of a VO_x ($x \approx 1$) ultrathin epitaxial film on Pt (111). Thin Solid Films 400(1–2):154–159. https://doi.org/10.1016/S0040-6090(01)01502-4
20. Schoiswohl J, Surnev S, Netzer FP et al (2006) Vanadium oxide nanostructures: from zero- to three-dimensional. J Phys: Condens Matter 18(4):R1–R14. https://doi.org/10.1088/0953-8984/18/4/R01
21. Barcaro G, Fortunelli A (2019) 2D oxides on metal materials: concepts, status, and perspectives. Phys Chem Chem Phys 21(22):11510–11536. https://doi.org/10.1039/c9cp00972h
22. Surnev S, Fortunelli A, Netzer FP (2013) Structure-property relationship and chemical aspects of oxide-metal hybrid nanostructures. Chem Rev 113(6):4314–4372. https://doi.org/10.1021/cr300307n
23. Schoiswohl J, Sock M, Eck S et al (2004) Atomic-level growth study of vanadium oxide nanostructures on Rh(111). Phys Rev B 69(15):1688. https://doi.org/10.1103/PhysRevB.69.155403
24. Schoiswohl J, Surnev S, Sock M et al (2005) Reduction of vanadium-oxide monolayer structures. Phys Rev B 71(16):86102. https://doi.org/10.1103/PhysRevB.71.165437
25. Hesse M, von Boehn B, Locatelli A et al (2015) Island ripening via a polymerization-depolymerization mechanism. Phys Rev Lett 115(13):136102. https://doi.org/10.1103/PhysRevLett.115.136102
26. von Boehn B, Penschke C, Li X et al (2020) Reaction dynamics of metal/oxide catalysts: methanol oxidation at vanadium oxide films on Rh(111) from UHV to 10^{-2} mbar. J Catal 385:255–264. https://doi.org/10.1016/j.jcat.2020.03.016
27. von Boehn B, Mehrwald S, Imbihl R (2018) Hole patterns in ultrathin vanadium oxide layers on a Rh(111) surface during catalytic oxidation reactions with NO. Chaos 28(4):45117. https://doi.org/10.1063/1.5020360
28. von Boehn B, Imbihl R (2018) Chemical wave patterns and oxide redistribution during methanol oxidation on a V-oxide promoted Rh(110) surface. J Phys Chem C 122(24):12694–12703. https://doi.org/10.1021/acs.jpcc.8b00852
29. von Boehn B, Menteş TO, Locatelli A et al (2018) Reactive phase separation during methanol oxidation on a V-oxide-promoted Rh(110) surface. J Phys Chem C 122(19):10482–10488. https://doi.org/10.1021/acs.jpcc.8b02544
30. von Boehn B, Imbihl R (2017) Large amplitude excitations traveling along the interface in bistable catalytic methanol oxidation on Rh(110). Phys Chem Chem Phys 19(28):18487–18493. https://doi.org/10.1039/c7cp01890h
31. von Boehn B, Preiss A, Imbihl R (2016) Dynamics of ultrathin V-oxide layers on Rh(111) in catalytic oxidation of ammonia and CO. Phys Chem Chem Phys 18(29):19713–19721. https://doi.org/10.1039/c6cp03637f
32. Tang Z, Wang S, Zhang L et al (2013) Effects of O_2 pressure on the oxidation of VO_x/Pt(111). Phys Chem Chem Phys 15(29):12124–12131. https://doi.org/10.1039/c3cp50712b
33. Petukhov M, Andrea Rizzi G, Granozzi G (2001) Ultrathin film growth and spectroscopic characterization of VO_x ($0.8 \leqslant x \leqslant 1.3$) on Pt(111). Surf Sci 490(3):376–384. https://doi.org/10.1016/s0039-6028(01)01356-5
34. Zheng Y, Zhang L, Wang S et al (2013) Synergistic effects of VO_x-Pt probed by the oxidation of propane on VO_x/Pt(111). Langmuir 29(29):9090–9097. https://doi.org/10.1021/la401256z
35. Levin M (1987) The enhancement of CO hydrogenation on rhodium by TiO_x overlayers. J Catal 106(2):401–409. https://doi.org/10.1016/0021-9517(87)90252-1
36. Boffa AB, Lin C, Bell AT et al (1994) Lewis acidity as an explanation for oxide promotion of metals: implications of its importance and limits for catalytic reactions. Catal Lett 27(3–4):243–249. https://doi.org/10.1007/BF00813909
37. Rodriguez JA, Liu P, Graciani J et al (2016) Inverse oxide/metal catalysts in fundamental studies and practical applications: a perspective of recent developments. J Phys Chem Lett 7(13):2627–2639. https://doi.org/10.1021/acs.jpclett.6b00499
38. Zhang J, Medlin JW (2018) Catalyst design using an inverse strategy: from mechanistic studies on inverted model catalysts to applications of oxide-coated metal nanoparticles. Surf Sci Rep 73(4):117–152. https://doi.org/10.1016/j.surfrep.2018.06.002
39. Tauster SJ (1987) Strong metal-support interactions. Acc Chem Res 20(11):389–394. https://doi.org/10.1021/ar00143a001
40. Tauster SJ, Fung SC, Garten RL (1978) Strong metal-support interactions. Group 8 noble metals supported on titanium dioxide. J Am Chem Soc 100(1):170–175. https://doi.org/10.1021/ja00469a029
41. Tauster SJ, Fung SC, Baker RT et al (1981) Strong interactions in supported-metal catalysts. Science 211(4487):1121–1125. https://doi.org/10.1126/science.211.4487.1121
42. Bernal S, Calvino JJ, Cauqui MA et al (2003) Some contributions of electron microscopy to the characterisation of the strong metal–support interaction effect. Catal Today 77(4):385–406. https://doi.org/10.1016/S0920-5861(02)00382-6
43. Liu JJ (2011) Advanced electron microscopy of metal-support interactions in supported metal catalysts. ChemCatChem 3(6):934–948. https://doi.org/10.1002/cctc.201100090
44. Shi XY, Zhang W, Zhang C et al (2016) Real-space observation of strong metal-support interaction: state-of-the-art and what's the next. J Microsc 262(3):203–215. https://doi.org/10.1111/jmi.12366
45. Willinger MG, Zhang W, Bondarchuk O et al (2014) A case of strong metal-support interactions: combining advanced microscopy and model systems to elucidate the atomic structure of interfaces. Angew Chem Int Ed Engl 53(23):5998–6001. https://doi.org/10.1002/anie.201400290
46. Penner S, Armbrüster M (2015) Formation of intermetallic compounds by reactive metal-support interaction: a frequently encountered phenomenon in catalysis. ChemCatChem 7(3):374–392. https://doi.org/10.1002/cctc.201402635
47. Shaikhutdinov S (2018) Strong metal-support interaction and reactivity of ultrathin oxide films. Catal Lett 148(9):2627–2635. https://doi.org/10.1007/s10562-018-2499-9
48. Campbell CT, Ertl G, Kuipers H et al (1981) A molecular beam study of the adsorption and desorption of oxygen from a Pt(111) surface. Surf Sci 107(1):220–236. https://doi.org/10.1016/0039-6028(81)90622-1
49. Brault P, Range H, Toennies JP (1997) Molecular beam studies of sticking of oxygen on the Rh(111) surface. J Chem Phys 106(21):8876–8889. https://doi.org/10.1063/1.473951
50. Parker DH, Bartram ME, Koel BE (1989) Study of high coverages of atomic oxygen on the Pt(111) surface. Surf Sci

217(3):489–510. https://doi.org/10.1016/0039-6028(89)90443-3
51. Yeo YY, Vattuone L, King DA (1997) Calorimetric heats for CO and oxygen adsorption and for the catalytic CO oxidation reaction on Pt{111}. J Chem Phys 106(1):392–401. https://doi.org/10.1063/1.473203
52. Getman RB, Xu Y, Schneider WF (2008) Thermodynamics of environment-dependent oxygen chemisorption on Pt(111). J Phys Chem C 112(26):9559–9572. https://doi.org/10.1021/jp800905a
53. Stranski IN, Krastanow L (1937) Zur Theorie der orientierten Ausscheidung von Ionenkristallen aufeinander. Monatsh Chem 71(1):351–364. https://doi.org/10.1007/BF01798103
54. Argile C, Rhead GE (1989) Adsorbed layer and thin film growth modes monitored by Auger electron spectroscopy. Surf Sci Rep 10(6–7):277–356. https://doi.org/10.1016/0167-5729(89)90001-0
55. Winkler A, Guo X, Siddiqui HR et al (1988) Kinetics and energetics of oxygen adsorption on Pt(111) and Pt(112)—a comparison of flat and stepped surfaces. Surf Sci 201(3):419–443. https://doi.org/10.1016/0039-6028(88)90495-5
56. Okamoto H (2009) Pt-V (Platinum-Vanadium). J Phase Equilib Diffus 30(6):666–667. https://doi.org/10.1007/s11669-009-9597-8
57. Smolinsky T, von Boehn B, Imbihl R (2018) Chemical waves in the O_2+H_2 reaction on a Rh(111) surface alloyed with nickel. I. Photoelectron emission microscopy. J Chem Phys 148(15):154704. https://doi.org/10.1063/1.5020372
58. Smolinsky T, Homann M, von Boehn B et al (2018) Chemical waves in the O_2+H_2 reaction on a Rh(111) surface alloyed with nickel. II. Photoelectron spectroscopy and microscopy. J Chem Phys 148(15):154705. https://doi.org/10.1063/1.5020381
59. Surnev S, Vitali L, Ramsey MG et al (2000) Growth and structure of ultrathin vanadium oxide layers on Pd(111). Phys Rev B 61(20):13945–13954. https://doi.org/10.1103/PhysRevB.61.13945
60. Kratzer M, Surnev S, Netzer FP et al (2006) Model reaction studies on vanadium oxide nanostructures on Pd(111). J Chem Phys 125(7):74703. https://doi.org/10.1063/1.2336770
61. Surnev S, Kresse G, Sock M et al (2001) Surface structures of ultrathin vanadium oxide films on Pd(111). Surf Sci 495(1–2):91–106. https://doi.org/10.1016/S0039-6028(01)01503-5
62. Kishi K, Fujiwara K (1997) The structures and chemical states of ultrathin vanadium oxides on Ni(110) surface studied by LEED and XPS. J Electron Spectrosc Relat Phenom 85(1–2):123–134. https://doi.org/10.1016/S0368-2048(96)03093-9
63. Dupuis A-C, Abu Haija M, Richter B et al (2003) V_2O_3 on Au and W: growth, termination and electronic structure. Surf Sci 539(1–3):99–112. https://doi.org/10.1016/S0039-6028(03)00752-0
64. Guimond S, Sturm JM, Göbke D et al (2008) Well-ordered V_2O_5(001) thin films on Au(111): growth and thermal stability. J Phys Chem C 112(31):11835–11846. https://doi.org/10.1021/jp8011156
65. Sturm JM, Göbke D, Kuhlenbeck H et al (2009) Partial oxidation of methanol on well-ordered V_2O_5(001)/Au(111) thin films. Phys Chem Chem Phys 11(17):3290–3299. https://doi.org/10.1039/b822384j
66. Ganduglia-Pirovano MV, Reuter K, Scheffler M (2002) Stability of subsurface oxygen at Rh(111). Phys Rev B. https://doi.org/10.1103/physrevb.65.245426
67. Mavrikakis M, Rempel J, Greeley J et al (2002) Atomic and molecular adsorption on Rh(111). J Chem Phys 117(14):6737–6744. https://doi.org/10.1063/1.1507104
68. Frank B, Fortrie R, Hess C et al (2009) Reoxidation dynamics of highly dispersed VO_x species supported on γ-alumina. Appl Catal A: Gen 353(2):288–295. https://doi.org/10.1016/j.apcata.2008.11.002
69. Carrero CA, Schloegl R, Wachs IE et al (2014) Critical literature review of the kinetics for the oxidative dehydrogenation of propane over well-defined supported Vanadium oxide catalysts. ACS Catal 4(10):3357–3380. https://doi.org/10.1021/cs5003417
70. Goodrow A, Bell AT (2007) A theoretical investigation of the selective oxidation of methanol to formaldehyde on isolated vanadate species supported on silica. J Phys Chem C 111(40):14753–14761. https://doi.org/10.1021/jp072627a
71. Khaliullin RZ, Bell AT (2002) A density functional theory study of the oxidation of methanol to formaldehyde over vanadia supported on silica, titania, and zirconia. J Phys Chem B 106(32):7832–7838. https://doi.org/10.1021/jp014695h
72. Kim HY, Lee HM, Metiu H (2010) Oxidative dehydrogenation of methanol to formaldehyde by a vanadium oxide cluster supported on rutile TiO_2(110): which oxygen is involved? J Phys Chem C 114(32):13736–13738. https://doi.org/10.1021/jp103361v
73. von Boehn B (2020) Redistribution dynamics of ultrathin vanadium oxide layers under catalytic conditions and activation of diffusion by surface acoustic waves. Doctoral Thesis, Leibniz University Hannover. https://doi.org/10.15488/9805
74. von Boehn B, Menteş TO, Locatelli A et al (2017) Growth of vanadium and vanadium oxide on a Rh(110) surface. J Phys Chem C 121(36):19774–19785. https://doi.org/10.1021/acs.jpcc.7b04809
75. Sambi M, Petukhov M, Domenichini B et al (2003) A photoelectron diffraction study of the surface-V_2O_3 (2×2) layer on Pd(111). Surf Sci 529(1–2):L234–L238. https://doi.org/10.1016/S0039-6028(03)00070-0
76. Todorova M, Reuter K, Scheffler M (2004) Oxygen overlayers on Pd(111) studied by density functional theory. J Phys Chem B 108(38):14477–14483. https://doi.org/10.1021/jp040088t